International Journal of the Physical Sciences Vol. 6(14), pp. 3336-3346, 18 July 2011
Available online at http://www.academicjournals.org/IJPS
DOI: 10.5897/IJPS11.447
ISSN 1992 - 1950 ©2011 Academic Journals

Full Length Research Paper

Improved hardness of laser alloyed X12CrNiMo martensitic stainless steel

D. I. Adebiyi[1]*, T. Fedotova[1], S. L. Pityana[1,2] and A. P. I. Popoola[1]

[1]Department of Chemical and Metallurgical Engineering, Tshwane University of Technology, P.M.B. X680, Pretoria, South Africa, 0001.
[2]Centre for Scientific and Industrial Research – National Laser Centre, P.O. Box 395, BLD 46F, Pretoria, South Africa, 0001.

Accepted 17 May, 2011

The improvement in hardness of X12CrNiMo martensitic stainless steel laser alloyed with 99.9% pure titanium carbide, stellite 6 and two cases of premixed ratio of titanium carbide and stellite 6 [TiC (30 wt.%)- stellite 6 (70 wt.%) and TiC (70 wt.%)- stellite 6 (30 wt.%)] were examined. The powders were supplied through a pneumatically driven powder delivery system with a 4.4 kW continuous wave (CW) Nd:YAG laser. The microstructures of the alloyed zones were investigated by x-ray diffractometer (XRD), energy dispersive spectroscopy (EDS) and scanning electron microscopy (SEM). The alloyed zones obtained by alloying with premixed ratio of 70 wt.% TiC and 30 wt.% stellite 6 were free from dilution and crack that were in those of pure stellite 6. A significant increase in Vickers hardness value compared with that of the substrate was achieved with the powders and their premixed ratios; 608 HVN for TiC and 503 HVN for stellite 6, 763 HVN for 30 wt.% TiC and 1025 HVN for 70 wt.% TiC.

Key words: Martensitic stainless steel, premixed ratio, alloyed zone, titanium carbide, stellite 6.

INTRODUCTION

The application of laser surface modification to prolong the service life of engineering components exposed to aggressive environments has gained increasing acceptance in recent years and material processing by laser beams has been well established as an advanced manufacturing technology.

Laser surface alloying (LSA), in which modification is achieved by localized melting, the deposition of a second powdery material into the melt pool, followed by solidification of a new alloy, is increasingly recognised as a powerful surface modification tool to enhance the surface property of engineering components (Thawari et al., 2003). LSA has attracted considerable attention in recent years as an efficient method to improve the chemical and mechanical surface properties of engineering components. The improvement in these properties by the LSA technique is achieved by introducing alloying materials into the laser-melted component surface, typically in the form of powder. The diverse choice of alloying materials that can be incorporated by this method ensures that the surface properties can be tailored to impart good wear, corrosion and oxidation properties to combat virtually any degradation mode (Thawari et al., 2003).

Martensitic stainless steels are widely used in manufacturing components with high mechanical properties and moderate corrosion resistance. As the properties of these steels can be changed by heat treatment, they are suitable for wide range of applications such as components of steam generators, pressure vessels, cutting tools, pump impellers, valves and turbines either in blades or shafts (Mahmoudi et al., 2010). However, the use of martensitic stainless steel (MSS) is limited because of low hardness; poor tribological behaviour and poor corrosion resistance due to the limitations in chromium and nickel content (Alexandre, 2009; Thamizhmanii et al., 2008; Yun-Tao et al., 2008).

According to Vamsi et al. (2004), the engineering solution to minimize or eliminate such surface initiated failure lies in tailoring the surface composition and/or microstructure of the near surface region without affecting the bulk properties. Hence, in recent times, the need for

*Corresponding author. E-mail: biyidammy@yahoo.co.uk; AdebiyiDI@tut.ac.za.

Table 1. The nominal chemical composition wt.% of the substrate and the powders.

Element	Fe	C	Si	Mn	P	Cr	Mo	Ni	V	N_2	Co	Nb	W	Ti
AR	Bal.	0.199	0.18	0.65	0.023	11.74	1.62	2.82	0.312	0.0381	-	-	-	-
TiC	-	27	-	-	-	-	-	-	-	-	-	-	-	73
Stellite 6	2.262	-	-	0.281	-	26.481	-	3.261	-	-	59.552	0.068	8.095	-

excellent properties in specific applications has led to the research of significant performance improvements of these steels (Calliari et al., 2008; Yun-tao et al., 2008).

Laser alloying has been successfully used to improve the hardness of MSS and various stainless steels by incorporating carbides (Adebiyi et al., 2010; Ayers et al., 1980; Marsden et al., 1986; Kim and Kim, 1992) and borides (Rieker et al., 1989). Vamsi et al. (2004) and Lo et al. (2003) agreed that martensitic stainless steel could have higher hardness values if the matrix is tailored to have a microstructure that is composed of martensite, retained austenite, and finer carbide. According to them, such microstructure will be suitable for resistance against erosion with favourable combination of strength and toughness.

According to Dong et al. (2009) and Chen and Wang (2006), TiC is a common carbide and has many excellent advantages, such as very high hardness (3200 HV), high melting point (~3100°C), low density (4.93 g/cm^3), low coefficient of friction and excellent thermal and chemical stability. As a result of these excellent properties, TiC is expected to be a suitable reinforcing phase for MSS.

Stellite 6 consists of complex carbides in an alloy matrix and has exceptional resistance to wear and many forms of mechanical and chemical degradation over a wide temperature range. Stelite 6 also retains a reasonable level of hardness up to 500°C and resists oxidation up to 1095°C. These properties are mainly due to the unique inherent characteristics of the hard carbide phase dispersed in a CoCr alloy matrix. Stellite 6 alloy is usually used for alloying due to its high hardness and good bonding strength with substrate (Sun et al., 2005).

However, heat build-up is high during laser alloying with stellite 6 using the continuous wave laser. This heat build-up usually leads to undesirable effects of high dilution and cracking of the alloyed layer (Sun et al., 2005). Ceramic powders such as TiC have relatively high absorptance of laser radiation (Candel et al., 2010) and could significantly minimize heat build-up in the work-piece.

It is therefore supposed that, the synthesis of a premixed ratio of TiC and stellite 6 is one possible solution to the problem of alloying with stellite 6. It is expected that alloying with such premixed ratio will significantly reduce the heat built-up in the test piece and therefore minimizes dilution and tendency to crack. Moreover, the composite coatings of such premixed ratio hold a promise of novel microstructure of fine carbide in the matrix of the MSS which will greatly improve the hardness of the steel.

The current investigation presents quantitative study of the improvement in hardness of different laser coatings. The effect of the reinforcement proportion (premixed ratio of TiC and stellite 6) on the hardness properties, the microstructures and phases of the resultant alloys are studied.

EXPERIMENT

Materials

The substrate is as-received 12Cr martensitic stainless steel (AR). The powders are stellite 6, commercially pure titanium carbide and two cases of premixed ratio of titanium carbide and stellite 6; [TiC (30 wt.%)-stellite 6 (70 wt.%) and TiC (70 wt.%) -stellite 6 (30 wt.%)]. The nominal chemical composition of the substrate and the powders are shown in Table 1.

The substrate was cut, machined to dimensions 100 x 100 x 6 mm; and sandblasted to clean the surface, minimize reflection of radiation during laser processing and enable the absorption of the laser energy. The phase composition of the powders were determined by Philips PW 1713 X-ray diffractometer fitted with monochromatic Cu K_α radiation set at 40 KV and 20 mA. The scan was taken between 10° and 80° 2 theta (2θ) and a step size of 0.02 degrees. The phase identification was done using Philips Analytical X'Pert HighScore® software with an inbuilt international centre for diffraction data (ICSD) database as the phase identifier. Scanning electron microscope and Malvern instrument Mastersizer 2000 were used to determine the morphology and size distribution of the powders.

Laser alloying

The alloying was performed with a 4.4 kW continuous wave (CW) Rofin Sinar Nd:YAG laser fitted with an off-axis nozzle for powder feeding. The powders were delivered at a mass flow rate of 3 L/min into the laser spot of 4 mm on the work piece. The molten piece was shrouded from the atmosphere by argon gas flowing at 3 L/min to prevent oxidation of the metal through reaction with oxygen, and also to avoid formation of pores due to excessive dissolution of nitrogen. Laser power and the scan speed were varied as shown in Tables 2 - 4.

Metallographic and microstructural characterisation

After laser alloying, the samples were cross-sectioned, polished, cleaned, dried and etched. TiC alloyed zone was etched with Kallings 2 reagent while stellite 6 alloyed zone was etched with Marble reagent. The microstructure was investigated by scanning electron microscopy and the phases present in the alloyed zone

Table 2. Processing parameters used for TiC alloying experiment.

Sample no.	System composition	Power (kW)	Scan speed (m/sec)	Beam diameter (mm)	Powder feed rate (rpm)	Shielding gas	Shielding gas flow rate (L/min)
1	MSS-TiC	2	0.016	4	3	Argon	3
2	MSS-TiC	2	0.014	4	3	Argon	3
3	MSS-TiC	2	0.012	4	3	Argon	3
4	MSS-TiC	2	0.010	4	3	Argon	3
5	MSS-TiC	3	0.016	4	3	Argon	3
6	MSS-TiC	3	0.014	4	3	Argon	3
7	MSS-TiC	3	0.012	4	3	Argon	3
8	MSS-TiC	3	0.010	4	3	Argon	3

Table 3. Processing parameters used for stellite 6 alloying experiment.

Sample no.	System composition	Power (kW)	Scan speed (m/sec)	Beam diameter (mm)	Powder feed rate (rpm)	Shielding gas	Shielding gas flow rate (L/min)
1	MSS-stellite 6	1.5	0.010	4	3	Argon	3
2	MSS-stellite 6	1.5	0.015	4	3	Argon	3
3	MSS-stellite 6	1.5	0.020	4	3	Argon	3
4	MSS-stellite 6	2.0	0.010	4	3	Argon	3
5	MSS-stellite 6	2.0	0.015	4	3	Argon	3
6	MSS-stellite 6	2.0	0.020	4	3	Argon	3

Table 4. Processing parameters used for the alloying experiment of the premixed ratio [TiC (30 wt. %)-stellite 6 (70 wt.%) and TiC (70 wt.%)-stellite 6 (30 wt.%)].

Sample no.	Power (kW)	Scan speed (m/sec)	Beam diameter (mm)	Powder feed rate (rpm)	Shielding gas	Shielding gas flow rate (L/min)
1	1.8	0.012	4	3	Argon	3
2	1.8	0.014	4	3	Argon	3
3	1.8	0.016	4	3	Argon	3

were determined by XRD using Cu K_{α} radiation.

Hardness test

The laser alloyed specimens were cross-sectioned and prepared for micro hardness investigation. The hardness measurements were performed on the prepared cross-section of the specimen with a Vickers hardness tester according to the ISO standard 3878 using a Matsuzawa Seiki. A Vickers hardness profile-indentation from the surface of the alloyed zone through to the substrate were measured at 100 µm interval between corresponding indentations using a load of 200 g.

RESULTS AND DISCUSSION

Materials characterisation

Figures 1 and 2 respectively show the XRD pattern of the TiC and stellite 6 powders used in the experiment. From Figures 1 and 2, it was observed that the powders were free from contamination, peaks showing only titanium and carbon in Figure 1. Each powder has an average particle size range of 45 to 100 µm. Figures 3 and 4 are the scanning electron micrographs of the powders. As shown in Figures 3 and 4, the morphologies of the TiC particles were granular and irregular in shape (Figure 3), while that of stellite 6 were round (Figure 4). The flow of powder particles during laser alloying is affected by the morphology of alloying powders. Round particles flow better than irregular ones during laser alloying. The EDS and x-ray spectra of the steel are respectively shown in Figures 5 and 6; its microhardness value is 300±0.4 HVN.

Composition and microstructure of the surface alloys

The XRD analyses of the alloyed layers revealed that the

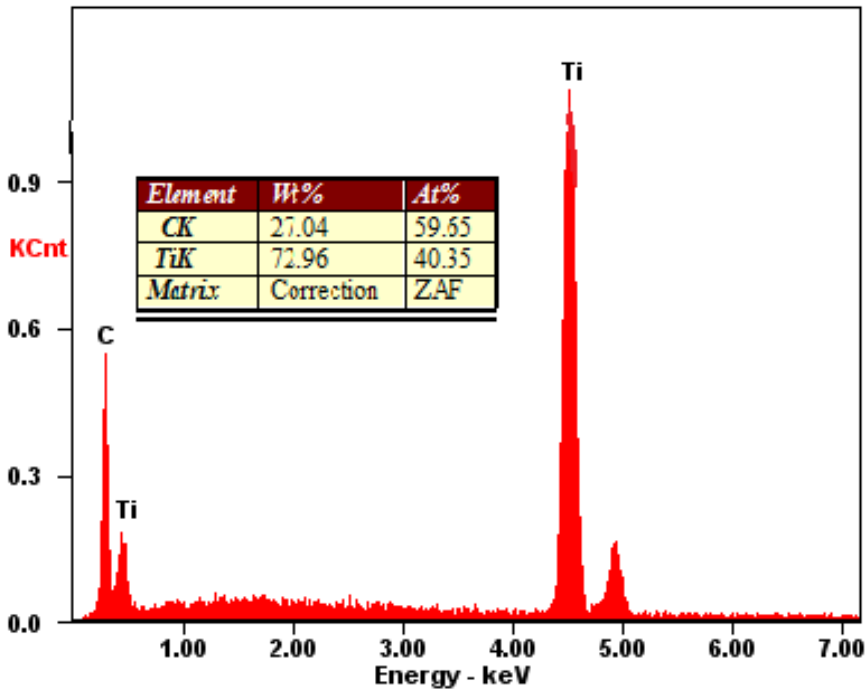

Figure 1. XRD pattern of the TiC powder.

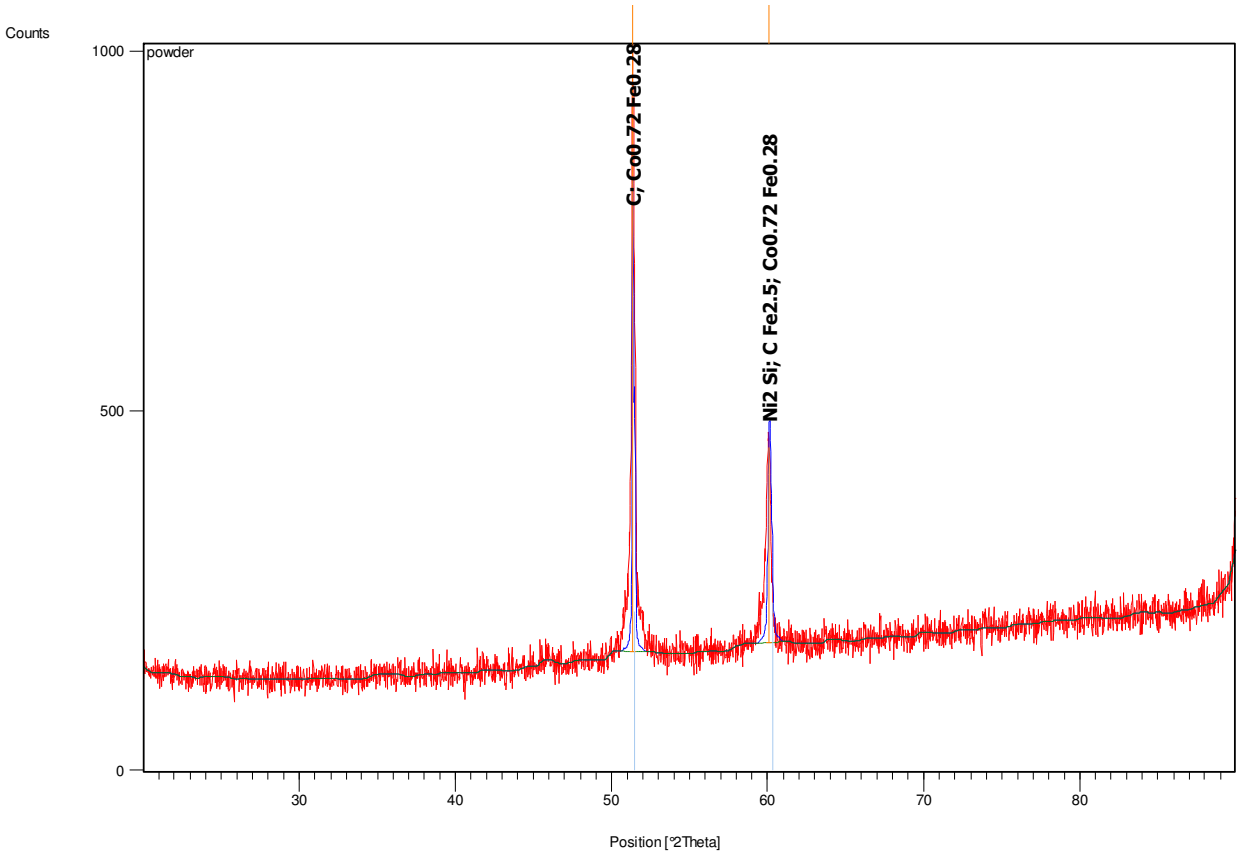

Figure 2. XRD pattern of the stellite 6 powder

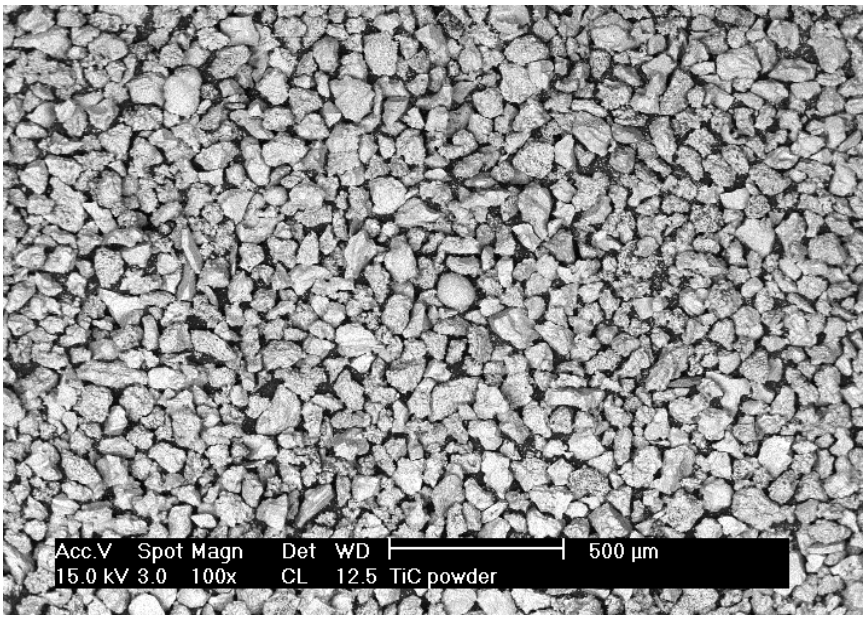

Figure 3. Scanning electron micrograph showing the morphology of the TiC powder.

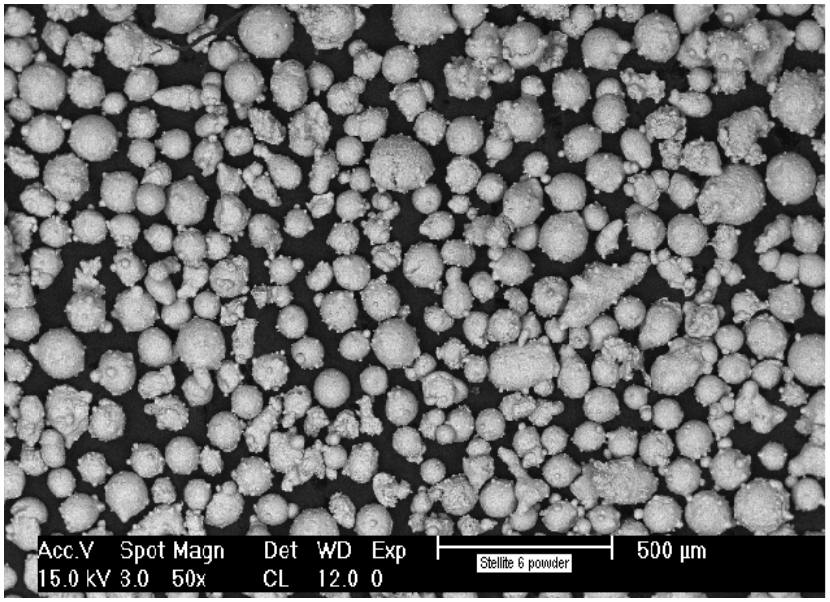

Figure 4. Scanning electron micrograph showing the morphology of the stellite 6 powder.

alloyed zones produced by the incorporation of TiC and stellite 6 powders and their premixed ratios into the matrix of the stainless steel yielded a variety of microstructures. The SEM of the alloyed zone produced by the incorporation of stellite 6 is shown in Figure 7. The XRD shows that the alloyed zone is composed of cobalt iron (Co_3Fe_7), chromium iron nickel (Ni - Cr - Fe), kamacite (Fe Ni) and chromium silicon (Cr Si_2). The XRD revealed that Hagg carbide (C_2Fe_5) and nickel silicon (Ni_2Si) present in the stellite 6 powder were absent in the alloyed zone, which provides a proof of their complete dissolution in the melt pool during the alloying process. However, traces of cobalt iron from the powder were found in the alloyed zone, showing that it did not completely dissolve in the melt pool.

The SEM of the TiC-MSS alloyed zone as shown in Figure 8 revealed a pore and crack free composite microstructure of TiC in martensite matrix with even distribution

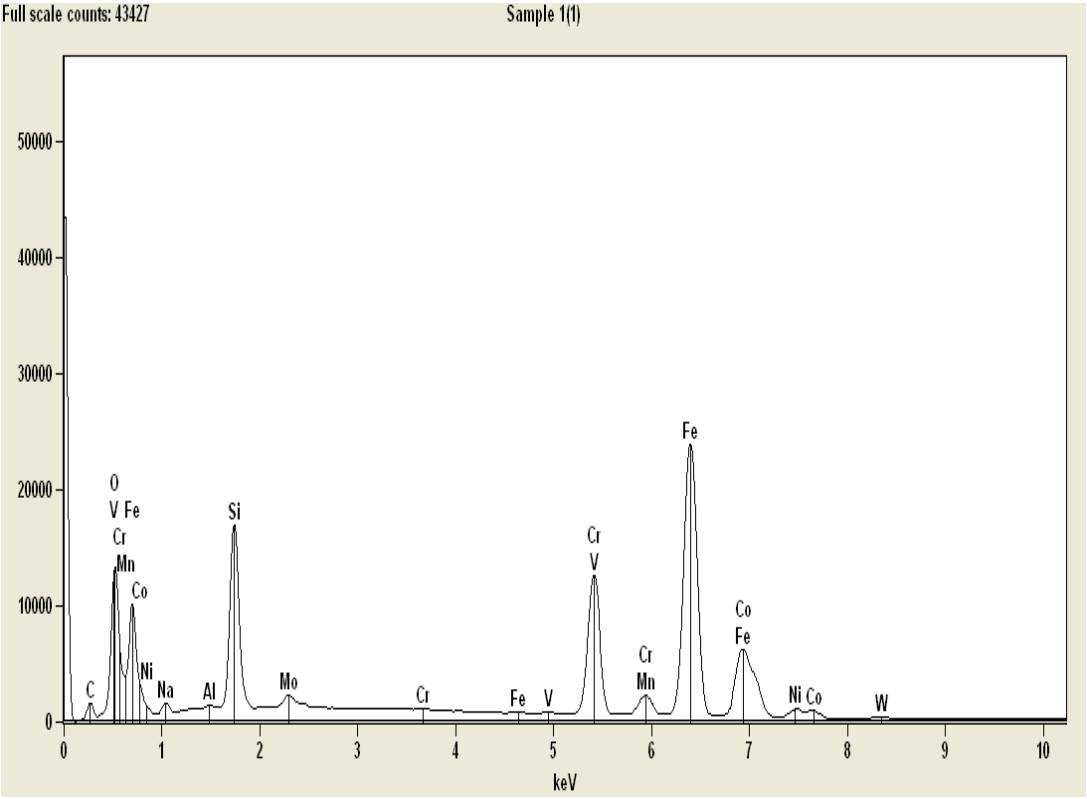

Figure 5. EDS of the matensitic stainless steel.

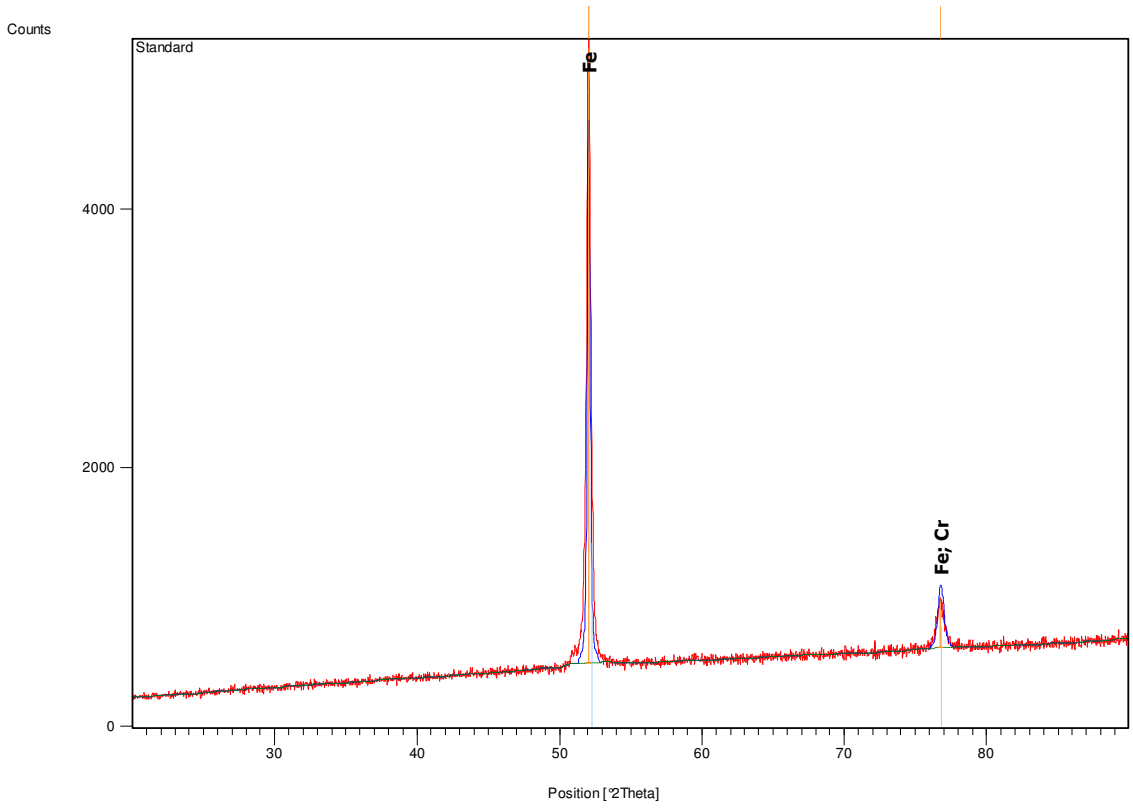

Figure 6. XRD of the matensitic stainless steel.

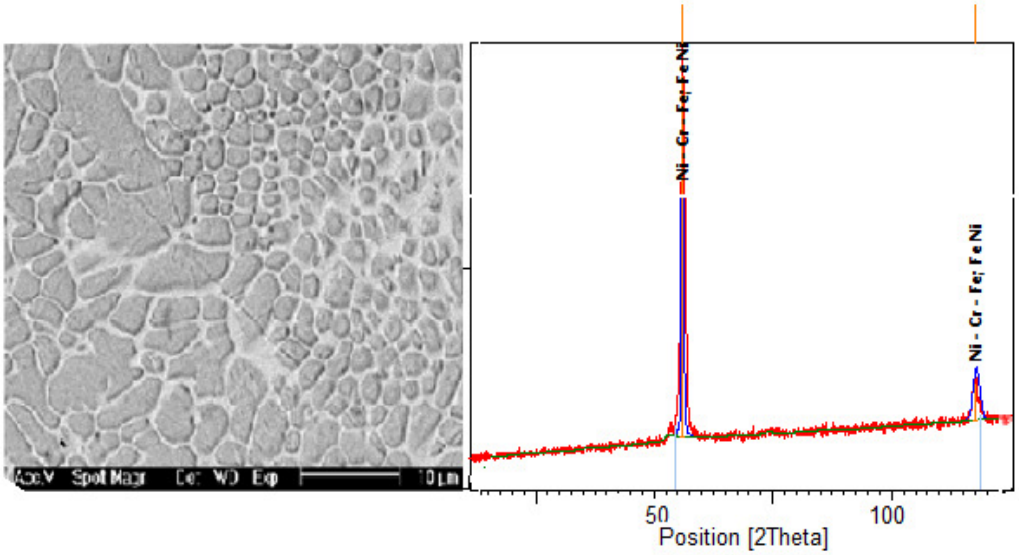

Figure 7. SEM and chemical composition of sample laser alloyed with stellite 6.

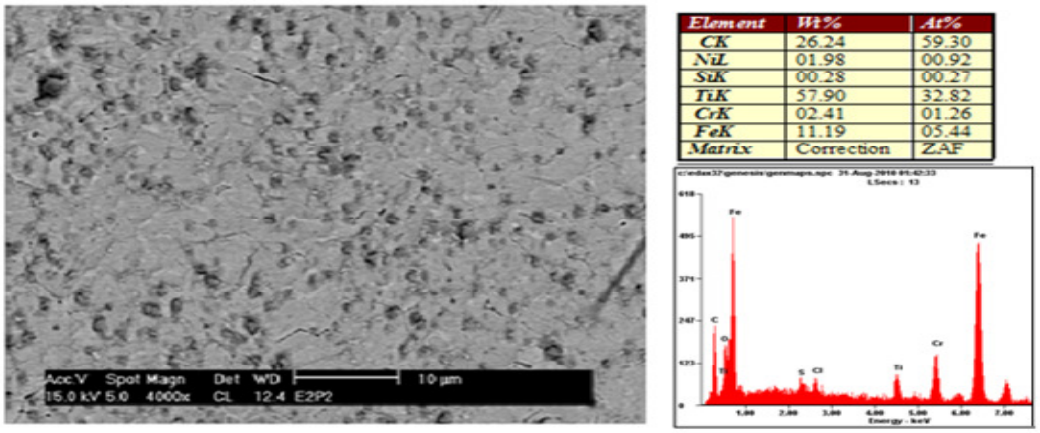

(a)

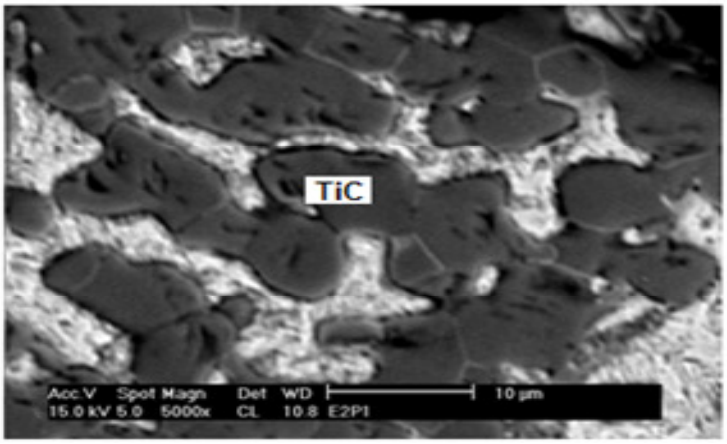

(b)

Figure 8. SEM and chemical composition of sample laser alloyed with TiC showing (a) fine even distribution of TiC and (b) coarse TiC in the matrix. (a) P = 3 KW, V = 0.14 m/min; (b) P = 2 KW, V = 0.01 m/min.

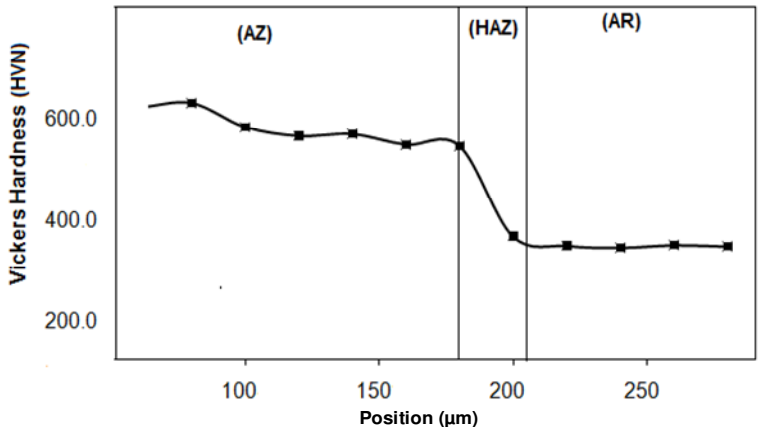

Figure 9. Typical microhardness profile of the samples alloyed with TiC showing (a) alloyed zone (AZ); (b) heat affected zone, (HAZ), and (c) the substrate, (AR).

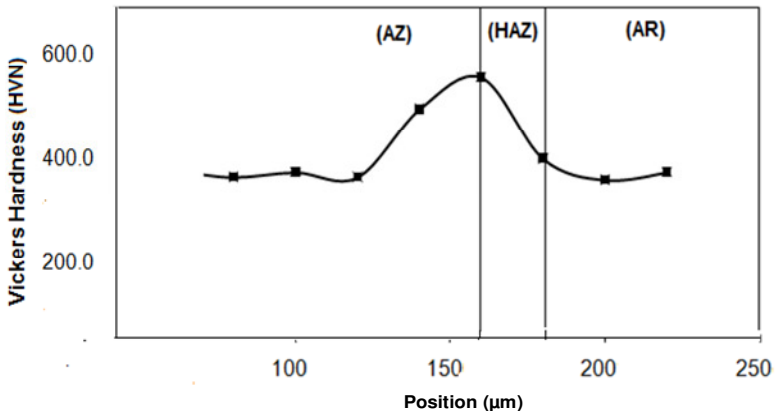

Figure 10. Typical hardness profile of the samples alloyed with stellite 6 showing (a) no increase in hardness until few millimetres into the alloyed zone (AZ), (b) the heat affected zone (HAZ) and (c) the substrate (AR).

distribution of carbides in the matrix of the MSS, which explain the dissolution of TiC in the MSS during laser irradiation. The microstructure of the TiC-MSS matrix shows dissolution and supersaturation of carbon in the steel matrix. As observed in the micrographs, carbide dissolution is higher when the scan speed is lower (Figure 8 (a)), the carbide becoming coarser with increased scanning speed (Figure 8 (b)). The higher carbide dissolution at lower scanning speed is probably due to higher energy per unit mass and interaction time between the laser beam and the substrate.

Hardness analysis

Figure 9 displays the typical microhardness depth profiles for samples alloyed with TiC. The microhardness was measured at the centerline of the alloyed zones from the alloyed surface into the substrate of the base metal. Although fluctuation in hardness value was observed for some of the samples few millimeters below the surface of the alloyed zone, all the samples showed a very significant overall increase in hardness in the alloyed zone (AZ). Maximum Vickers hardness of 648 VHN was obtained in the alloyed zone (AZ), which gradually decreased to 300 VHN in the unaltered matrix (AR). These hardness test results indicated that the hardness of the alloyed zone increased more than two times that of the unaltered matrix. This increase is probably due the presence of TiC particles at the metal-ceramic interface as this interface influences the structure and mechanical properties of the composite. Although few clusters of TiC particles were seen in the composite, there is however a homogeneous distribution of the TiC grains in the matrix, and this usually enhances isotropic properties in the matrix. Typical hardness profile of the alloyed layer measured along the depth from the irradiated surface for the samples alloyed with stellite 6 is shown in Figure 10.

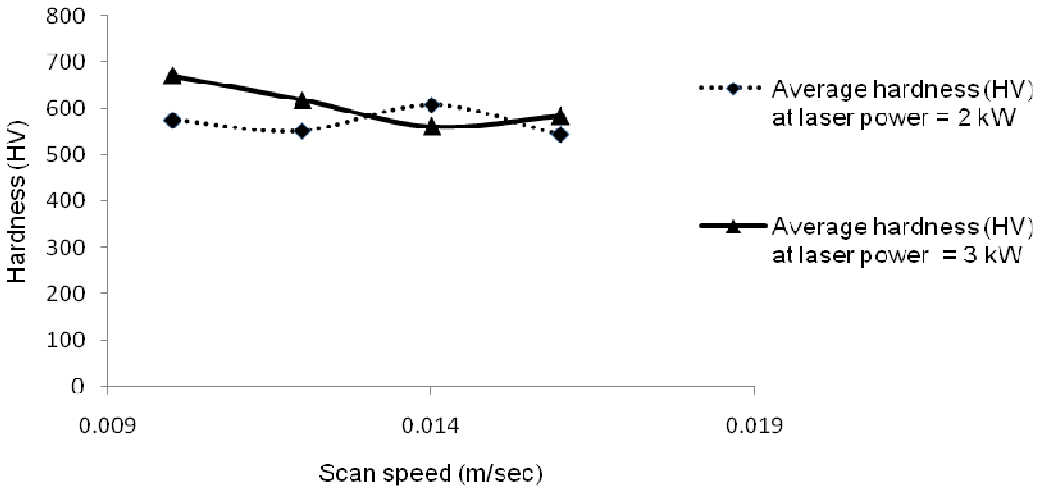

Figure 11. Average hardness of TiC alloyed samples at various scan speed and laser power.

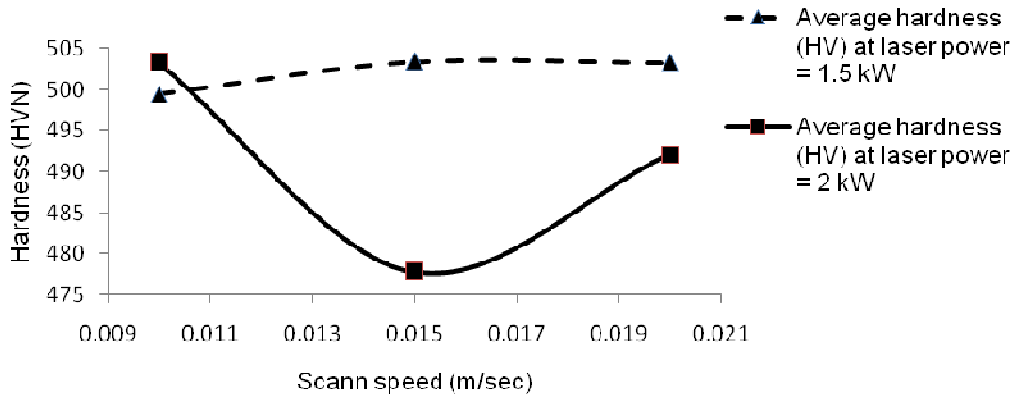

Figure 12. Average hardness of stellite 6 alloyed samples at various scan speed and laser powers.

In all the samples, increase in hardness is not observed until the region of about 100 µm below the surface of the alloyed layer. This is probably due to dilution. Although there are few cracks in the alloyed zone, maximum hardness of 503 HVN is observed in this zone. The mechanism of the improvement in hardness of stellite 6 alloyed layers is attributed to the formation of metal carbide M_7C_3 and the metastable $M_{23}C_6$, and the presence of DO_{19} hcp supperlattice structure Co_3W precipitates (Sun et al., 2005). This significant increase in hardness of stellite 6 alloyed layer is due to solid solution hardening, precipitation strengthening, dislocation–dislocation interactions and impenetrable particle hardening.

The variation of average hardness with laser power and scan rate for both powders are shown in Figures 11 and 12. For the TiC, at a relatively high laser power, the hardness diminished with increased scanning speed. This is probably due to insufficient time for the powder to react sufficiently with the matrix. The alloyed layer of the premixed ratio generally have higher hardness values compared with that of the pure powders (100%) of TiC and stellite 6, (Figure 13). The highest hardness observed in the premixed ratio of TiC (70 wt.%)-stellite 6 (30 wt.%). This is probably due to higher proportion of the carbide phase in the premix ratio of 70 wt.% TiC as shown in Figure 14. Unlike that of the 100 wt.% stellite 6, the layer produced by alloying the X12CrNiMo substrate with the premixed ratio is good and the cross section is crack free. The layer of the premixed ratio has a maximum hardness of about 1025 HVN. This increase in hardness is due to the higher percentage of the titanium carbide and undissolved carbide. The presence of the undissolved carbide is attributed to the higher melting point of TiC (3140°C) compared to that of Ni (1453°C), Cr (1875°C), and Mo (2623°C) contents of the steel. Hence, during laser irradiation, any of the constituent elements Ni, Cr and Mo would have melted before the TiC particle could melt (Figure 14).

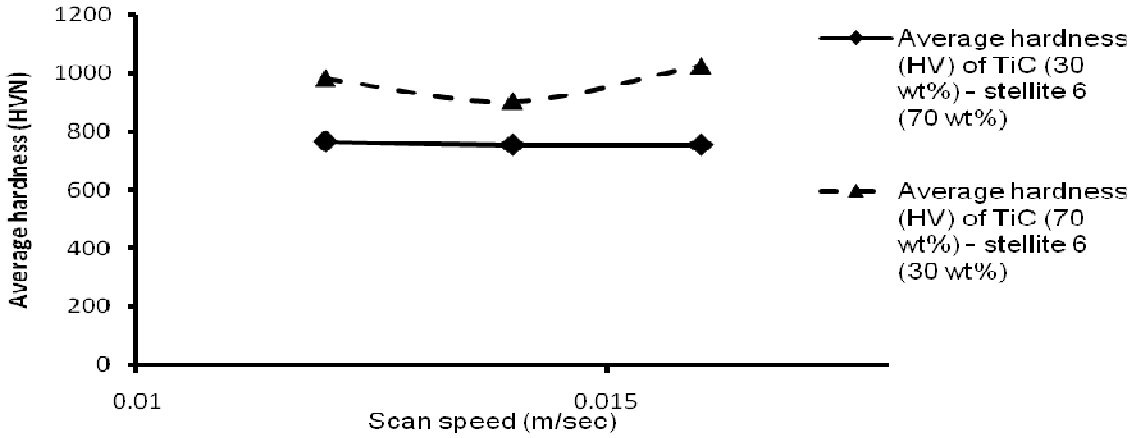

Figure 13. Average hardness of premix ratio of TiC and stellite 6.

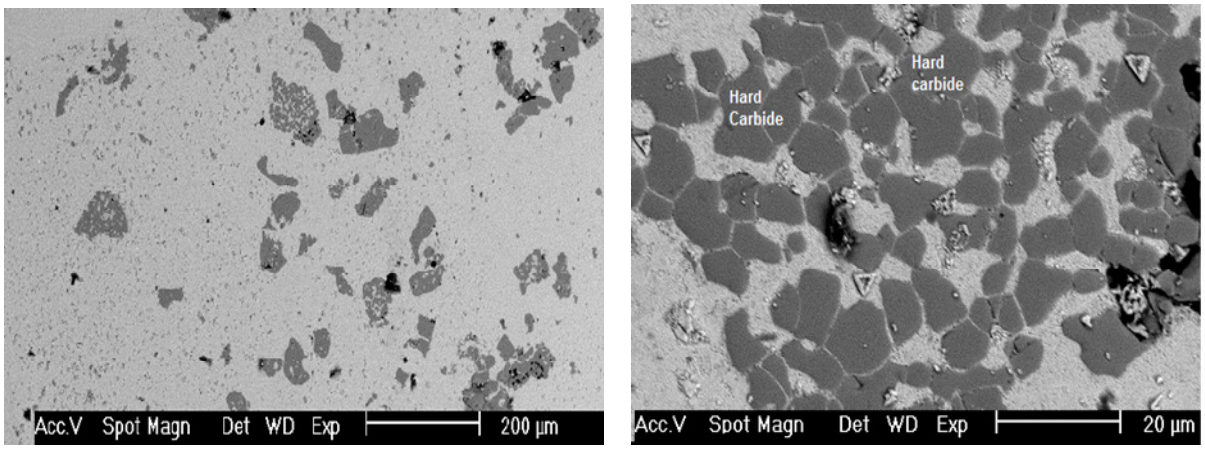

Figure 14. SEM micrographs showing microstructure of surface alloyed with: (a) premixed ratio of 30 wt. % TiC +70 wt. % stellite 6, (b) premixed ratio of 70 wt. % TiC + 30 wt. % stellite 6. The SEM shows that (b) contains greater proportion of the hard carbide phase.

Conclusion

In this study, X12CrNiMo martensitic stainless steel was laser alloyed with TiC, stellite 6 and premixed ratio of both powders using a CW Nd:YAG laser. The micro-structural evolution and hardness of the alloyed zones were investigated and the following were established:

- X12CrNiMo martensitic stainless steel was successfully alloyed with TiC, stellite 6 and premixed ratio of TiC and stellite 6. Uniform dispersion of the powders into the matrix of the substrate, good metallurgical bonding and a defect free alloyed zones were obtained with the TiC and the premixed ratios of TiC and stellite 6;
- The alloyed zone produced by the incorporation of TiC is composed of fine carbide and martensite. The microstructure of the TiC-MSS matrix shows dissolution and supersaturation of carbon in the steel matrix. It was observed that carbide dissolution is higher when the scan speed is lower, the carbide becoming coarser with increased scanning speed.

The alloyed zone produced by the incorporation of stellite 6 is composed of Cobalt Iron (Co_3Fe_7), Chromium Iron Nickel (Ni - Cr - Fe), Kamacite (Fe Ni) and Chromium Silicon ($CrSi_2$). Complete dissolution of both the Hagg carbide (C_2Fe_5) and Nickel silicon (Ni_2Si) in the powder took place.

- Laser alloying with both TiC and stellite 6 greatly improved the microhardness of the alloyed zone to about 648 and 503 HVN, respectively in comparison to about 300 HVN for the substrate.
- Unlike those of the 100 wt.% stellite 6, the layers produced

by alloying with the premixed ratio are good and the cross sections are crack free.

- The alloyed layers produced by the premixed ratio generally have higher hardness values compared with those of the pure powders of TiC and stellite 6.The premixed ratio of TiC (70 wt.%)-stellite 6 (30 wt.%) has the highest hardness of more than 150% of the substrate. The more the TiC, the higher the hardness values obtained.

REFERENCES

Adebiyi DI, Popoola AP, Ogunniyi IO (2010). Hardness and microstructure of X12CrNiMo martensitic stainless steel laser alloyed with titanium carbide. 55th Annual conference of the South African Institute of Physics, ISBN: 978-0-620-46211-2.

Alexandre VL, Bincoletol, Davis ML, Frederico APF, Luiz CC, Pedro APN (2009). Surface modification of the AISI 410 martensitic stainless steel by plasma nitriding. XXX CBRAVIC.

Ayers JD, Tucker TR (1980). Particulate-TiC-hardened steel surfaces by laser melt injection. Thin solid films, 73 (1): 201-207.

Calliari I, Zanesco M, Dabala M, Brunelli K, Ramous E (2008). Investigation of microstructure and properties of a Ni–Mo martensitic stainless steel. Mat. Design, 29: 246–250.

Candel JJ, Amigó V, Ramos JA, Busquets D (2010). Sliding wear resistance of TiC_p reinforced titanium composite coating produced by laser cladding. Surf. Coatings Tech., 204: 3161–3166.

Chen Y, Wang HM (2006). Microstructure and wear resistance of laser-melted TiC reinforced nickel aluminide dual-phase matrix in situ composite. Intermetallics, 14: 325–331.

Dong YJ, Wang HM (2009). Microstructure and dry sliding wear resistance of laser clad TiC reinforced Ti–Ni–Si intermetallic composite coating. Surf. Coatings Tech., 204: 731–735.

Kim TH, KIM BC (1992). Chromium carbide laser-beam surface-alloying treatment on stainless steel. J. Mat. Sci., 27(11): 2967-2973.

Lo KH, Cheng FT, MAN HC (2003). Laser transformation hardening of AISI 440c martensitic stainless steel for higher cavitation erosion resistance. Surf. Coatings Tech., 173:96-104.

Mahmoudi B, Torkamany MJ, Sabour AR, Sabbaghzade J (2010). Laser surface hardening of AISI 420 stainless steel treated by pulse N: YAG laser. Mat. Design, 31: 2553-2560.

Marsden C, West DRF, Steen WM (1986). L*a*ser surface treatment of metals. *E*: 461.

Rieker C, Morris DG, Steffen J (1989). Formation of hard microcrystalline layers on stainless steel by laser alloying. Mat. Sci. Tech., 5: 590-594.

Sun S, Durandet Y, Brandt M (2005). Parametric investigation of pulsed Nd: YAG laser cladding of stellite 6 on stainless steel. Surf. Coatings Tech., 194: 225– 231.

Thawari G, Sundararajan G, Joshi SV (2003). Laser surface alloying of medium carbon steel with $SiC_{(P)}$. Thin Solid Films, 423: 41–53.

Thamizhmanii S, Bin OB, Saparudin S, Hasan S (2008). Surface roughness analyses on hard martensitic stainless steel by turning. J. Ach. in Mat. Manuf. Eng., 26: 2.

Vamsi CB, Krishna MM, Satya P (2004). Surface modification of martensitic stainless steel using metal working Co_2 laser. Int. Symp. Research Students Mat. Sci. Eng., pp. 1-13.

Yun-Tao X, Dao-xin L, Dong H (2008). Improvement of corrosion and wear resistances of AISI 420 martensitic stainless steel using plaa nitriding at low temperature. Surf. Coatings Tech., 202: 2577–2583.